

Inelastic neutron scattering study of crystal field levels in $\text{PrOs}_4\text{As}_{12}$

Songxue Chi,¹ Pengcheng Dai,^{1,2} T. Barnes,^{1,2} H. J. Kang,³ J. W. Lynn,³ R. Bewley,⁴ F. Ye,² M. B. Maple,⁵ Z. Henkie,⁶ and A. Pietraszko⁶

¹*Department of Physics and Astronomy, The University of Tennessee, Knoxville, Tennessee 37996-1200, USA*

²*Oak Ridge National Laboratory, Oak Ridge, Tennessee 37831, USA*

³*NIST Center for Neutron Research, National Institute of Standards and Technology, Gaithersburg, Maryland 20899-6102, USA*

⁴*Rutherford Appleton Laboratory, Chilton, Didcot, Oxon OX11 0QX, United Kingdom*

⁵*Department of Physics, University of California at San Diego, La Jolla, California 92093, USA*

⁶*Institute of Low Temperature and Structure Research, Polish Academy of Science, 50-950 Wrocław, Poland*

(Received 16 January 2008; revised manuscript received 27 January 2008; published 25 March 2008)

We use neutron scattering to study the Pr^{3+} crystalline electric field (CEF) excitations in the filled skutterudite $\text{PrOs}_4\text{As}_{12}$. By comparing the observed levels and their strengths under neutron excitation with the theoretical spectrum and neutron excitation intensities, we identify the Pr^{3+} CEF levels and show that the ground state is a magnetic $\Gamma_4^{(2)}$ triplet, and the excited states Γ_1 , $\Gamma_4^{(1)}$, and Γ_{23} are at 0.4, 13, and 23 meV, respectively. A comparison of the observed CEF levels in $\text{PrOs}_4\text{As}_{12}$ with the heavy fermion superconductor $\text{PrOs}_4\text{Sb}_{12}$ reveals the microscopic origin of the differences in the ground states of these two filled skutterudites.

DOI: 10.1103/PhysRevB.77.094428

PACS number(s): 75.47.-m, 71.70.Ch

I. INTRODUCTION

The Pr-based filled skutterudites (FSs) have the formula $\text{PrT}_4\text{X}_{12}$, where T is one of the transition metals Fe, Ru, or Os, and X is a pnictogen (P, As, or Sb).¹⁻³ The notably mounting interests and efforts in the study of the FS compounds are motivated by the remarkable diversity of their electronic and magnetic ground states, including multipole ordering,^{4,5} small gap insulators,^{6,7} conventional superconductivity,⁸ unconventional superconductivity,^{9,10} and magnetic ordering.¹¹⁻¹⁵ Despite the large differences in their physical properties, these compounds are governed by only a few parameters, including the interaction between the conduction and the $4f$ shell electrons (the c - f coupling) and the effect of the crystalline electric field (CEF) potential on the Pr^{3+} $4f$ electrons.⁴⁻¹⁵ For example, transport and bulk magnetic measurements on the heavy fermion superconductor $\text{PrOs}_4\text{Sb}_{12}$ suggested either a Γ_1 singlet ground state or a Γ_3 nonmagnetic doublet ground state.^{9,10} Inelastic neutron scattering experiments on $\text{PrOs}_4\text{Sb}_{12}$ showed that the Pr^{3+} CEF levels include a Γ_1 singlet ground state and a low-lying $\Gamma_4^{(2)}$ magnetic triplet excited state at 0.6 meV.¹⁷⁻¹⁹ This rules out the quadrupolar Kondo effect, which arises only from a nonmagnetic doublet ground state,¹⁶ as the microscopic origin for the observed heavy fermion superconductivity.

The FS compounds belong to the space group $Im\bar{3}$.³ The rare earth atoms are located at the corners and body center of the cubic lattice, each of which is surrounded by a simple cube of 8 transition metal atoms at the $8c$ sites [Fig. 1(a)] and by an icosahedron of 12 pnictogen atoms at the 24g Wyckoff sites [Fig. 1(c)]. Owing to their unique structure, a subtle modification on composition can result in a different CEF scheme and thus a completely different ground state. However, a general understanding is desirable as to how the compositions influence the CEF levels. In $\text{PrOs}_4\text{As}_{12}$, in which the pnictogen Sb in $\text{PrOs}_4\text{Sb}_{12}$ is replaced by As, the

material displays quite different correlated electron properties.^{13,14} The temperature dependence of the electrical resistivity reveals Kondo lattice behavior, which is not observed in $\text{PrOs}_4\text{Sb}_{12}$.²⁰ Specific heat measurements indicate an enhanced electronic specific heat coefficient of $\gamma \approx 1$ J/mol K² for $T \leq 1.6$ K and $0 \leq H \leq 1.25$ T.¹³ The compound exhibits several ordered phases at temperatures below 2.3 K and fields below about 3 T.²¹ The ground state has been determined to be antiferromagnetic (AF) by neutron scattering experiments.¹⁴ A determination of the Pr^{3+} CEF level scheme in $\text{PrOs}_4\text{As}_{12}$ and its microscopic origin is crucial for understanding why its ground state is different from that in $\text{PrOs}_4\text{Sb}_{12}$. The outcome will lead to a more general understanding of how the structures and compositions in Pr-based FSs can influence their CEF levels and ground states.

II. EXPERIMENT

$\text{PrOs}_4\text{As}_{12}$ single crystals were grown using the molten metal flux method described in Ref. 13 and crushed into fine powder. Our neutron scattering experiments were carried out on the cold neutron triple-axis spectrometer SPINS at the NIST Center for Neutron Research (NCNR) and on the HET chopper spectrometer at ISIS (Rutherford Appleton Laboratory), as described previously.²² We reference positions in reciprocal space at wave vector $\mathbf{Q}=(q_x, q_y, q_z)$ in \AA^{-1} using (H, K, L) reciprocal lattice units notation, where $(H, K, L) = (q_x a/2\pi, q_y a/2\pi, q_z a/2\pi)$ for the cubic $\text{PrOs}_4\text{As}_{12}$ cell ($a = 8.5319$ \AA).¹³ We used a ³He-⁴He dilution refrigerator for the field-dependent experiments. The nature of observed CEF excitations were confirmed in large temperature (0.08–200 K) and magnetic field (0–11 T) ranges.

III. RESULTS AND DISCUSSION

Figure 2 summarizes the neutron scattering intensity from $\text{PrOs}_4\text{As}_{12}$ on HET at temperatures between 1.5 and 200 K.

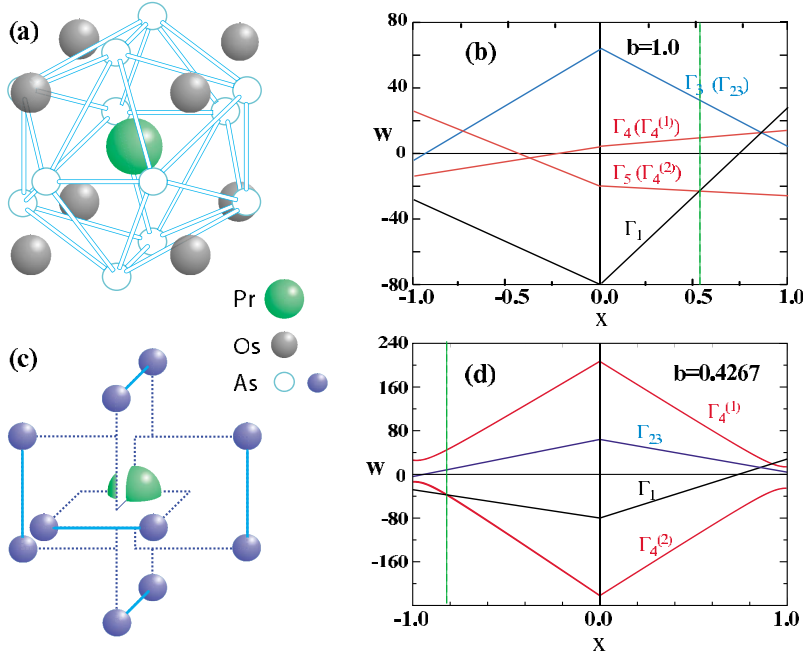


FIG. 1. (Color online) (a) The cube of eight Os ions surrounding the central Pr^{3+} ion in $\text{PrOs}_4\text{As}_{12}$. These give an O_h -symmetric CEF. (b) The corresponding spectrum of O_h -symmetry Pr^{3+} CEF levels. (black: singlet; blue (dark gray): doublet; red (light gray): triplet). The relative coupling x that gives singlet-triplet degeneracy is shown by the dashed vertical. (c) The 12 nearest neighbor As ions surrounding the central Pr^{3+} in $\text{PrOs}_4\text{As}_{12}$, giving a reduced symmetry (T_h) CEF. (d) The corresponding As-only T_h -symmetry Pr^{3+} CEF spectrum in $\text{PrOs}_4\text{As}_{12}$. Here, W and x are the same as defined by Ref. 25.

Since the CEF magnetic scattering decreases with increasing Q whereas the intensity of phonons increases with Q , a comparison of the neutron intensities in the low- and high-angle detectors can distinguish between magnetic and phonon scatterings. Figure 2(a) shows the scattering function at $T = 1.5$ K and $T = 200$ K with an incident neutron beam energy of $E_i = 32$ meV. Comparison of the low- and high-angle data reveals two clear CEF excitations at 13 and 23 meV, with

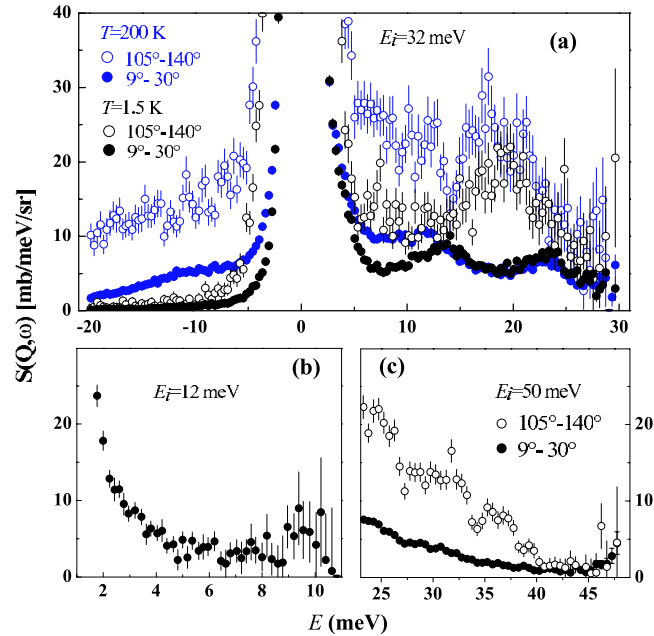


FIG. 2. (Color online) (a) Neutron inelastic scattering at $T = 1.5$ K (black circles) and $T = 200$ K (blue/gray circles) with $E_i = 32$ meV, integrated over scattering angles from 9° to 30° (low-angle detectors) and from 105° to 140° (high-angle detectors). (b) The same at $E_i = 12$ meV; (c) $E_i = 50$ meV. The scattering function $S(Q, \omega)$ was normalized by comparison to a vanadium standard.

phonons at ~ 20 meV. Measurements with $E_i = 12$ and 50 meV showed no evidence of additional CEF excitations at energy transfers between 2 and 8 meV or above 25 meV [Figs. 2(b) and 2(c)].

To search for CEF excitations at energies below 2 meV, we carried out high resolution measurements using SPINS. At $T = 0.32$ K, energy scans at $Q = (1.2, 0, 0)$ showed a clear peak at 0.4 meV; this mode decreases and becomes broader on warming to 2.5 and 6 K [Fig. 3(a)]. Figure 3(b) shows that the energy of the ~ 0.4 meV mode is the weak Q dependence and decreases in intensity with increasing Q , thus confirming its magnetic nature. Figure 3(d) reveals that the elastic intensity also decreases on warming from 0.08 to 4 K. This reduction of intensity in the elastic channel with increasing temperature is also observed in the HET data, evidencing that the ground state is a magnetic multiplet.

Figures 4(a)–4(d) show the temperature dependence of the low-angle scattering for $E_i = 32$ meV. The CEF peak intensities do not change significantly with temperature between 1.5 and 5 K. At 50 K, the intensity in the elastic channel has undergone a substantial decrease, and the 13 meV peak has shifted to 10 meV. On further increasing the temperature to 100 and 200 K, the intensities at 0, 13, and 23 meV continue to decrease, whereas the scattering at 10 meV increases.

The theoretical description of the Pr^{3+} CEF levels in $\text{PrOs}_4\text{As}_{12}$ is complicated by the presence of important contributions from two sets of neighboring ions, Os and As. The Pr^{3+} ion in Pr-based FS has a $4f^2$ configuration, which in Russell–Saunders coupling has a ninefold degenerate 3H_4 ground state. This degeneracy is lifted by the CEF interaction, which we assume to be dominated by the 12 nearest neighbor pnictogens (As) and the 8 next nearest neighbor Os ions; the distances to these ions are $d_{\text{Pr-As}} = 3.23$ Å and $d_{\text{Pr-Os}} = 3.69$ Å.

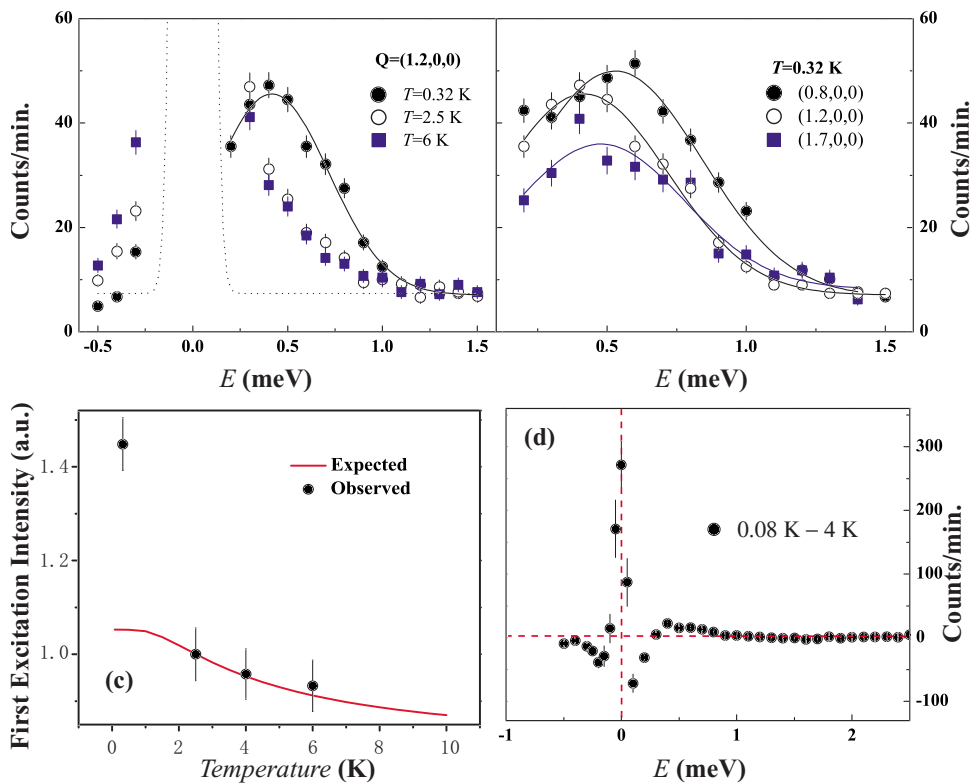


FIG. 3. (Color online) (a) Low energy spectrum of CEF excitations observed at $T=0.32$, 2.5, and 6.0 K using the SPINS spectrometer at NCNR. (b) The wave vector dependence of the excitations at $Q=(0.8,0,0)$, $Q=(1.2,0,0)$, and $Q=(1.7,0,0)$. (c) The expected and observed temperature dependences of the intensity of the 0.4 meV mode. (d) The temperature difference spectrum between 0.08 and 4 K, showing clear reduction in magnetic elastic scattering.

A. Single-charge model with separate ions

Os ions form a simple cube around the Pr ions and they alone give an O_h symmetric CEF. The arrangement of the 12 pnictogens (As) around Pr^{3+} forms three orthogonally intersected planes where the As-As bonds are shown as solid lines with length L and W is the length of the dashed lines in Fig. 1(c) ($b=W/L=0.4267 \neq 1$). When the four pnictogen atoms in each of the three orthogonally intersected planes form a square, i.e., $b=W/L=1$, the fourfold rotational symmetry is recovered and the point group symmetry becomes O_h with the simple cubic CEF potentials [Fig. 1(c)].²⁵ This

O_h case is treated by Lea *et al.*²⁵ (see their Fig. 9); we have rederived their excitation spectrum as shown in Fig. 1(b).

Both O_h and T_h CEF interactions split the $\text{Pr}^{3+} 3H_4$ ground state into a singlet, a doublet, and two triplets.²⁴ In the $b \neq 1$ T_h -symmetry case, these multiplets are referred to as Γ_1 (a singlet), Γ_{23} (a nonmagnetic doublet), and $\Gamma_4^{(1)}$ and $\Gamma_4^{(2)}$ (magnetic triplets). These two triplets are linear combinations of the O_h -symmetry triplets, mixed by the new T_h CEF interaction;²⁴ this mixing modifies the excitation spectrum and leads to b -dependent neutron transition intensities.

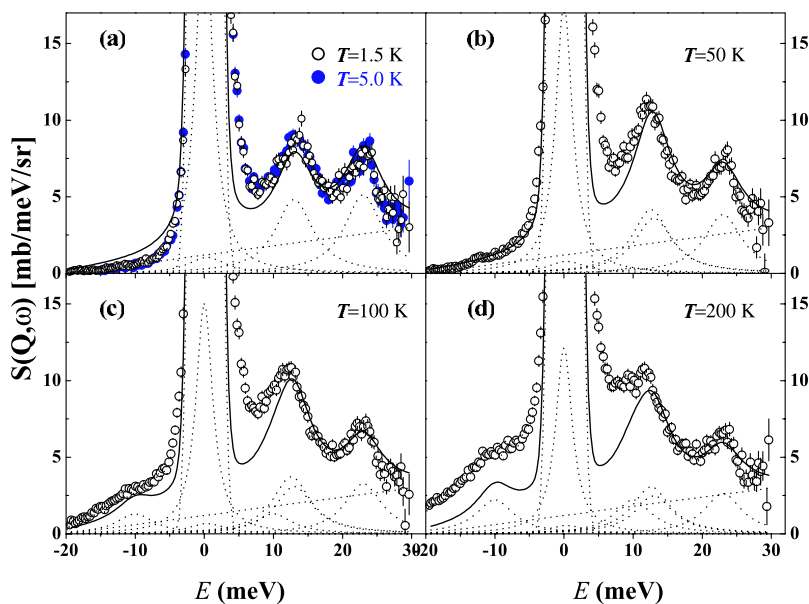


FIG. 4. (Color online) The temperature dependence of the excitations observed on HET with $E_i=32$ meV at (a) $T=1.5$, 5 K, (b) 50 K, (c) 100 K, and (d) 200 K. The lines are theoretical results for neutron excitation intensities, from the combined Os-As CEF model, with an arbitrary overall scale factor.

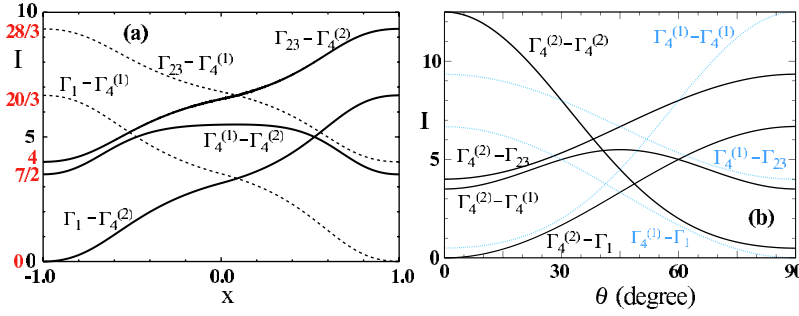


FIG. 5. (Color online) (a) The theoretical neutron transition intensity for As CEF alone with $b=0.4267$. (b) Neutron excitation intensities predicted by the combined Os-As CEF model.

The T_h -symmetry CEF excitation spectrum has not been considered in detail in the literature, and the corresponding neutron transition intensities between T_h CEF levels have not been considered at all. To aid in the interpretation of our neutron scattering data, we carried out these CEF calculations using a point charge model. We assumed an expansion of the perturbing CEF potential in spherical harmonics,

$$V(\Omega) = \sum_{\ell=4,6} g_{\ell} \sum_{m=-\ell}^{\ell} M_{\ell m} Y_{\ell m}(\Omega), \quad (1)$$

where the interaction strengths g_4 and g_6 are treated as free parameters. The spherical harmonic moments $\{M_{\ell m}\}$ are determined by the positions of the 12 As ions, which we assigned the (scaled) coordinates $\vec{x}=(\pm 1, \pm b, 0)$, $(0, \pm 1, \pm b)$, $(\pm b, 0, \pm 1)$. The nonzero independent moments for $\ell=4,6$ are $M_{40}=21(1-3b^2+b^4)/2\sqrt{\pi}(1+b^2)^2$, $M_{60}=3\sqrt{13}(2-17b^2+2b^4)/8\sqrt{\pi}(1+b^2)^2$, and $M_{66}=-15\sqrt{3003}b^2(1-b^2)/16\sqrt{\pi}(1+b^2)^3$. The nonzero M_{66} for $b \neq 1$ (T_h symmetry) confirms the presence of the B_1^6 terms of Takegahara *et al.* [Eq. (7) of Ref. 24], in addition to the usual B_c^4 and B_c^6 O_h -symmetry terms. (Note that the T_h -allowed moment M_{66} vanishes at the O_h -symmetry point $b=1$.) We also confirmed that the other nonzero moments satisfy the ratios quoted in Eq. (7) of Ref. 24. Unlike Takegahara *et al.*,²⁴ we do not introduce a new parameter y for the T_h -symmetry terms because they are completely determined by g_6 and the lattice parameter b in the point charge model. This was previously noted by Goremychkin *et al.*¹⁷

Diagonalization of this T_h CEF interaction within the $\text{Pr}^{+3} 3\text{H}_4$ nonet gives our results for the spectrum of CEF levels and their associated eigenvectors. These eigenvectors depend only on the ratio g_6/g_4 and the lattice parameter b ; the energies in addition have an arbitrary overall scale. Our results for the spectrum for $b=1$ (O_h symmetry) and $b=0.4267$ ($\text{PrOs}_4\text{As}_{12}$ geometry) are shown in Figs. 1(b) and 1(d), using the Lea-Leask-Wolf (LLW) normalization conventions.²⁵ [These conventions set our two Hamiltonian parameters in Eq. (1) to $g_4=(968\pi/21)x$ and $g_6=(-5808\pi/221)(1-|x|)$.] Note that the $b=1$ and $b=0.4267$ level schemes differ qualitatively, which demonstrates the importance of the T_h terms in this problem.

We find that the O_h singlet and doublet energy eigenvectors are unmodified by the T_h interaction, consistent with Takegahara *et al.*²⁴ The singlet eigenvector (in a J_z^{tot} basis) is $|\Psi_1\rangle=\sqrt{7/12}|0\rangle+\sqrt{5/24}(|4\rangle+|-4\rangle)$ and the two doublet states are $|\Psi_{23a}\rangle=-\sqrt{5/12}|0\rangle+\sqrt{7/24}(|4\rangle+|-4\rangle)$ and $|\Psi_{23b}\rangle$

$=\sqrt{1/2}(|2\rangle+|-2\rangle)$, consistent with earlier (numerical) results.^{24,25} The singlet and doublet energy eigenvalues in our conventions are modified by the T_h interaction. In terms of the LLW variable x (Ref. 25) and our parameter b , they are $E_1=-[16/13(1+b^2)^2][91x(1-3b^2+b^4)-20(1-|x|)(2-17b^2+2b^4)]$ and $E_{23}=-[16/13(1+b^2)^2][13x(1-3b^2+b^4)+16(1-|x|)(2-17b^2+2b^4)]$. The corresponding analytic results for the two T_h triplet states for general b are quite complicated, so we only present numerical results for these states.

The neutron transition intensities are defined by $I_{if}=|\langle f|J_z^{\text{tot}}|i\rangle|^2$, as introduced by Birgeneau.²⁶ (There is an implicit sum over initial and final magnetic quantum numbers.) Our T_h -symmetry results for these quantities are shown in Fig. 5(a). The values in the limits $x=\pm 1$ (no $\ell=6$ term, hence O_h symmetry) implicitly check Birgeneau's numerical O_h results; see the off-diagonal entries in his Table 1(e). These O_h limits are indicated on the vertical axis of Fig. 5(a).

Next, we compare the observed CEF levels and their neutron excitation intensities to the well-known LLW CEF results for O_h symmetry [Fig. 1(b)] and our calculated CEF predictions for $\text{PrOs}_4\text{As}_{12}$ under T_h symmetry [Figs. 1(d) and 5(a)]. Both O_h and T_h CEF spectra have x values that can accommodate a magnetic triplet ground state and a nearly degenerate singlet first excited state [vertical lines in Figs. 1(b) and 1(d)]. However, it is evident that the O_h scheme cannot explain the data because the observed 0.4 meV transition $\Gamma_4^{(2)} \rightarrow \Gamma_1$ is incorrectly predicted to have zero intensity due to the O_h symmetry. While in the T_h scheme the relative neutron excitation strengths of the higher levels (at 13 and 23 meV) predicted in Fig. 1(d) seem to be in good agreement with observation at low temperatures, the As CEF alone predicts an incorrect spectrum of levels [Fig. 1(d)], with the triplet $\Gamma_4^{(1)}$ being the highest excitation. The calculated neutron transition intensity shown in Fig. 5(a) cannot explain the observed intensity at higher temperatures. As temperature increases, the excited states get populated and the excitations from the ground state at 13 and 23 meV start to decrease in intensities. Meanwhile, the new excited-state transitions start to increase. If $\Gamma_4^{(1)}$ instead of Γ_{23} is the highest level, the intensity at 12.6 meV would not increase but that at 22.6 meV would because the Γ_1 to Γ_{23} transition is not allowed even in T_h symmetry. Goremychkin *et al.*¹⁷ showed that the highest level in the same Sb material is the Γ_{23} doublet.

B. Combined Os-As crystalline electric field model

The twin constraints of having the Γ_{23} level at the top of the spectrum and having a large $\Gamma_4^{(2)} \leftrightarrow \Gamma_1$ neutron excitation

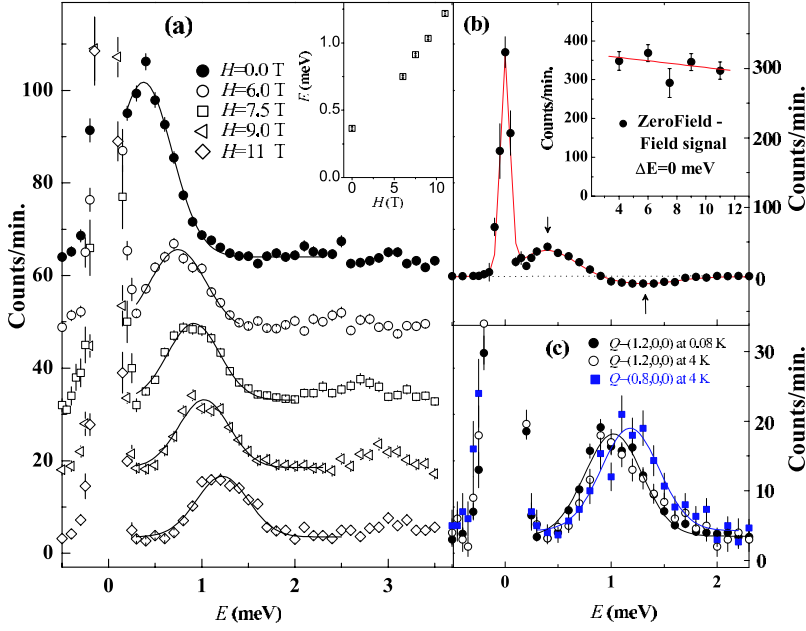


FIG. 6. (Color online) (a) The magnetic field dependence of the low-lying CEF excitations at $Q=(1.2,0,0)$ and $T=0.08$ K. The inset shows the field dependence of the first excited state. (b) The difference spectrum between 0 and 11 T at $Q=(1.2,0,0)$ and $T=0.08$ K. The effect of an applied field is to suppress intensity at $\hbar\omega=0$ meV and to split the spin-triplet ground state; the latter results in the field dependence of the 0.4 meV peak in (a), which may involve an intratriplet transition. The elastic intensity suppression effect essentially disappears for fields above 4 T. (c) The field-induced CEF excitation at ≈ 1.1 meV is weakly wave vector dependent and shows essentially no temperature dependence between $T=0.08$ and 4 K.

strength requires both Os and As terms in the CEF interaction. We therefore introduce a combined Os-As Hamiltonian,

$$H = H(\text{Os}) + H(\text{As}). \quad (2)$$

Although this model nominally has four parameters (g_4^{Os} , g_6^{Os} , g_4^{As} , and g_6^{As}), only three are independent; g_4^{Os} and g_4^{As} cannot be distinguished because they are summed into a single coefficient of the O_h -symmetry $\ell=4$ interaction. For this reason, we introduce combined O_h -symmetry Os-As coefficients $g_4 = g_4^{\text{Os}} + g_4^{\text{As}}$ and $g_6 = g_6^{\text{Os}} + g_6^{\text{As}}$, which we normalize according to LLW conventions. As the $\ell=6$ T_h -symmetry terms from $H(\text{As})$ in the CEF are proportional to g_6^{As} alone, the strengths g_6^{Os} and g_6^{As} can be distinguished. We parametrize these two $\ell=6$ interactions using the total O_h -symmetry g_6 and a T_h/O_h relative strength r_6 , which is the ratio of the coefficients of Y_{62} to Y_{60} in the CEF potential. The energy levels of this Hamiltonian are $E_{4(2)} = -6g_4 - 8g_6 - f$, $E_1 = 28g_4 - 80g_6$, $E_{4(1)} = -6g_4 - 8g_6 + f$, and $E_{23} = 4g_4 + 64g_6$, where $f = [(20g_4 + 12g_6)^2 + 960r_6^2 g_6^2]^{1/2}$. For $r_6=0$, these reduce to the familiar LLW O_h spectrum. In the pure As model, r_6 is determined by CEF theory if we assume point As ions and is given by $(11\sqrt{105}/4)b^2(1-b^2)/(1+b^2)[1-(17/2)b^2+b^4]$. For $\text{PrOs}_4\text{As}_{12}$, we have $b=0.4267$, which gives a rather large $r_6 = -6.901$. This drives strong level repulsion between the two triplets, which explains why the pure As spectrum of Fig. 1(d) differs so greatly from the O_h -symmetry (pure Os) spectrum of Fig. 1(b).

Our experimentally observed CEF levels are close to but not exactly consistent with the predictions above of the mixed Os-As model since the gap ratio $(E_{4(1)} - E_{4(2)}) / (E_{23} - E_{4(2)}) \approx 0.57$ is slightly below the theoretical lower bound of $7/12$. The parameters we estimate from the measured gaps are $g_4 \approx 0.24$ meV and $g_6 \approx 0.20$ meV. The value of r_6 is not determined by the measured energies due to the inconsistency mentioned above, although $r_6 \lesssim 0.5$ appears

plausible. A more sensitive determination of r_6 is possible through the measurement of the inelastic neutron excitation intensities we discuss below.

The neutron excitation intensities in this combined Os-As Hamiltonian depend only on a single parameter θ , which is the mixing angle of the triplet energy eigenvectors when expanded in an O_h -symmetry $|3\rangle, |3'\rangle$ basis,

$$|4(1)\rangle = +\sin(\theta)|3\rangle + \cos(\theta)|3'\rangle,$$

$$|4(2)\rangle = +\cos(\theta)|3\rangle - \sin(\theta)|3'\rangle. \quad (3)$$

This mixing angle is related to the Hamiltonian parameters by $\tan(2\theta) = 2\sqrt{15}r_6/[5(g_4/g_6)+3]$. The singlet and doublet O_h energy eigenvectors are unchanged. The nonzero neutron excitation intensities in terms of $s = \sin(\theta)$ and $c = \cos(\theta)$ are $\Gamma_4^{(2)} \leftrightarrow \Gamma_1 = (20/3)s^2$, $\Gamma_4^{(2)} \leftrightarrow \Gamma_4^{(1)} = 7/2 + 8c^2s^2$, $\Gamma_4^{(2)} \leftrightarrow \Gamma_{23} = 4 + (16/3)s^2$, $\Gamma_1 \leftrightarrow \Gamma_4^{(1)} = (20/3)c^2$, $\Gamma_4^{(1)} \leftrightarrow \Gamma_{23} = 28/3 - (16/3)s^2$, $\Gamma_4^{(2)} \leftrightarrow \Gamma_4^{(2)} = (25/2)(1 - (4/5)s^2)^2$, and $\Gamma_4^{(1)} \leftrightarrow \Gamma_4^{(1)} = (1/2)(1 + 4s^2)^2$. The calculated neutron scattering intensity of different transitions as a function of θ is shown in Fig. 5(b). We recover the O_h -symmetry results of Birgeneau [Table 1(e) of Ref. 26] for $s=0$, $c=1$.

We carried out a least-squares fit of our neutron excitation data at 1.5, 50, 100, and 200 K (Fig. 4) to the theoretical intensities given above, which gives an estimate of the triplet mixing angle θ in $\text{PrOs}_4\text{As}_{12}$,

$$\theta \approx 22.5^\circ. \quad (4)$$

When combined with the values of g_4 and g_6 from the spectrum, this θ corresponds to $r_6 \approx 1.2$. In this fit, the relatively isolated $\Gamma_4^{(2)} \rightarrow \Gamma_4^{(1)}$ peak at 23 meV was used to infer the background, which was taken to be constant plus linear. The assumed line shapes were Lorentzians with a common linewidth, fixed by the 23 meV peak. The calculated intensities of the individual transitions (dotted lines) and the total intensity (solid lines) for each temperature are shown in Figs.

4(a)–4(d). We note that the intensity reduction at 0.4 meV on warming from 0.32 to 2.5 K is larger than that expected from the CEF model [Fig. 3(c)], thus suggesting that Pr-Pr interactions below T_N ($=2.3$ K) are important. On the other hand, the large difference between the calculated and expected intensities around 8 meV in the 200 K data is presumably due to thermally populated phonons [Fig. 2(a)].

C. Field effect on the crystalline electric field gap

If the ground state of $\text{PrOs}_4\text{As}_{12}$ is indeed the $\Gamma_4^{(2)}$ triplet, application of a magnetic field should Zeeman split it, resulting in a field-dependent energy gap. There should also be a reduction in the intensity of the zero-energy $\Gamma_4^{(2)} \rightarrow \Gamma_4^{(2)}$ magnetic scattering. Figure 6 shows that these expectations are indeed qualitatively satisfied. The first excited state at 0.4 meV shifts toward higher energies as the applied field increases. The field-dependent transition energy is linear only at higher fields (between 6 and 11 T). The drop of intensity in the elastic channel is almost constant for all applied fields, as shown in the inset of Fig. 6(b). Figure 6(c) shows that the wave vector dependence is also present with applied magnetic field ($H=9$ T). Normally, the field splitting of the ground state multiplet would be a very clear test of our $\Gamma_4^{(2)}$ triplet assignment for the ground state. However, $\text{PrOs}_4\text{As}_{12}$ is complicated by the near degeneracy of the $\Gamma_4^{(2)}$ and Γ_1 levels, which mix strongly under an applied field. This results in a more complicated spectrum of low-lying states, with several low-field level crossings and neutron scattering intensities that are also modified by their field-induced $\Gamma_4^{(2)}-\Gamma_1$ mixing.

Our determination of the CEF levels in $\text{PrOs}_4\text{As}_{12}$ reveals the reasons for the wide range of behaviors in different FSs. The spectrum of CEF levels is largely determined by the O_h symmetry field of the eight nearest neighbor ions, and for Os, the near equality of the $\ell=4$ and $\ell=6$ strengths g_4 and g_6 implies nearly degenerate low-lying singlet (insulator) and triplet (AF) levels. The low temperature magnetic properties are determined by which of these phases happens to be the true ground state. In the CEF model, this is specified by the two parameters g_4/g_6 and r_6 (Fig. 7); in $\text{PrOs}_4\text{As}_{12}$, which has a triplet ground state, we estimate $g_4/g_6 \approx 1.15$ and $r_6 \approx 1.2$. The T_h symmetry pnictogen CEF (proportional to r_6) acts to stabilize the triplet state and can itself lead to a triplet ground state if r_6 is sufficiently large to cross the phase boundary shown in Fig. 7.

In principle, one can extend our approach to calculate the ground states of other Pr FSs by determining its crystal structure and g_4/g_6 ratio. The necessity of using the T_h symmetry of As rather than the O_h symmetry of pure Os form to explain the observed excitations shows that the detailed pnictogen geometry is important in determining the CEF levels.

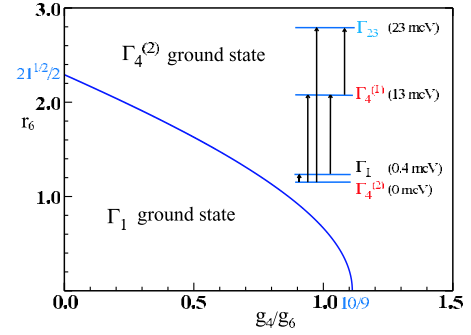


FIG. 7. (Color online) The boundary between singlet and triplet ground states in skutterudites ($E_1=E_4^{(2)}$) as a function of r_6 and g_4/g_6 and the observed $\text{PrOs}_4\text{As}_{12}$ spectrum.

Indeed, the AF-ordered ground state in $\text{PrOs}_4\text{As}_{12}$ can arise from a $\Gamma_4^{(2)}$ triplet magnetic ground state, while the superconducting $\text{PrOs}_4\text{Sb}_{12}$ has a nonmagnetic Γ_1 singlet ground state. The nearly degenerate first excited state Γ_1 at 0.4 meV (~ 4 K) and its temperature and field dependences (Figs. 4 and 6) may explain the presence of multiple transitions in the specific heat [in $C(T)/T$ versus T] and its field dependence.^{13,14,21}

IV. SUMMARY

To understand the observed Pr^{3+} CEF levels, one must incorporate the As ions' contribution to the CEF Hamiltonian,^{23,24} in addition to the usual Os cubic field terms. A comparison of our CEF calculations using this more general Hamiltonian with our experimental results shows that the Pr^{3+} CEF level scheme in $\text{PrOs}_4\text{As}_{12}$ consists of a $\Gamma_4^{(2)}$ magnetic triplet ground state, a nearly degenerate Γ_1 singlet excitation, and higher $\Gamma_4^{(1)}$ magnetic triplet and Γ_{23} nonmagnetic doublet excited states. We find that contributions in the CEF Hamiltonian due to As are important in determining the neutron excitation intensities in $\text{PrOs}_4\text{As}_{12}$; our results differ qualitatively from the predictions of the conventional CEF Hamiltonian,^{25,26} and therefore provide a microscopic understanding for its AF ground state.

ACKNOWLEDGMENTS

We thank R. J. Birgeneau, B. C. Sales, and D. Schultz for helpful discussion. The work at UT/ORNL was supported by the U.S. DOE under Grant No. DE-FG02-05ER46202. ORNL is managed by UT-Battelle, LLC, for the U.S. DOE under Contract No. DE-AC05-00OR22725. Work at UCSD was supported by the U.S. DOE under Grant No. DE-FG02-04ER46105 and by the NSF under Grant No. DMR-0335173. Work on SPINS was supported in part by the National Science Foundation under agreement No. DMR-0454672.

- ¹G. S. Nolas and G. Fowler, *Annu. Rev. Mater. Sci.* **29**, 89 (1999).
- ²B. C. Sales, in *Handbook on the Physics and Chemistry of Rare Earths*, edited by K. A. Gschneidner, Jr., J.-C. G. Bünzli, and V. K. Pecharsky (Elsevier Science, New York, 2003), Vol. 33, Chap. 211, pp. 1–34.
- ³B. C. Chakoumakos and B. C. Sales, *J. Alloys Compd.* **407**, 87 (2006).
- ⁴Y. Aoki, T. Namiki, T. D. Matsuda, K. Abe, H. Sugawara, and H. Sato, *Phys. Rev. B* **65**, 064446 (2002).
- ⁵H. Sugawara, T. D. Matsuda, K. Abe, Y. Aoki, H. Sato, S. Nojiri, Y. Inada, R. Settai, and Y. Ōnuki, *Phys. Rev. B* **66**, 134411 (2002).
- ⁶C. Sekine, T. Uchiumi, I. Shirovani, and T. Yagi, *Phys. Rev. Lett.* **79**, 3218 (1997).
- ⁷M. Matsunami, L. Chen, H. Okamura, T. Nanba, C. Sekine, and I. Shirovani, *J. Magn. Magn. Mater.* **272-276**, E39 (2004).
- ⁸M. Yogi, H. Kotegawa, Y. Imamura, G.-q. Zheng, Y. Kitaoka, H. Sugawara, and H. Sato, *Phys. Rev. B* **67**, 180501 (2003); N. Takeda and M. Ishikawa, *J. Phys. Soc. Jpn.* **69**, 868 (2000).
- ⁹E. D. Bauer, N. A. Frederick, P.-C. Ho, V. S. Zapf, and M. B. Maple, *Phys. Rev. B* **65**, 100506(R) (2002).
- ¹⁰M. B. Maple, E. D. Bauer, V. S. Zapf, E. J. Freeman, N. A. Frederick, and R. P. Dickey, *Acta Phys. Pol. B* **32**, 3291 (2001).
- ¹¹E. Bauer, S. Berger, C. Paul, M. Della Mea, G. Hilscher, H. Michor, M. Reissner, W. Steiner, A. Grytsiv, P. Rogl, and E. W. Scheidt, *Phys. Rev. B* **66**, 214421 (2002).
- ¹²N. P. Butch, W. M. Yuhasz, P.-C. Ho, J. R. Jeffries, N. A. Frederick, T. A. Sayles, X. G. Zheng, M. B. Maple, J. B. Betts, A. H. Lacerda, F. M. Woodward, J. W. Lynn, P. Rogl, and G. Giester, *Phys. Rev. B* **71**, 214417 (2005).
- ¹³W. M. Yuhasz, N. P. Butch, T. A. Sayles, P.-C. Ho, J. R. Jeffries, T. Yanagisawa, N. A. Frederick, M. B. Maple, Z. Henkie, A. Pietraszko, S. K. McCall, M. W. McElfresh, and M. J. Fluss, *Phys. Rev. B* **73**, 144409 (2006).
- ¹⁴M. B. Maple, N. P. Butch, N. A. Frederick, P.-C. Ho, J. R. Jeffries, T. A. Sayles, T. Yanagisawa, W. M. Yuhasz, Songxue Chi, H. J. Kang, J. W. Lynn, Pengcheng Dai, S. K. McCall, M. W. McElfresh, M. J. Fluss, Z. Henkie, and A. Pietraszko, *Proc. Natl. Acad. Sci. U.S.A.* **103**, 6783 (2006).
- ¹⁵D. T. Adroja, J.-G. Park, E. A. Goremychkin, N. Takeda, M. Ishikawa, K. A. McEwen, R. Osborn, A. D. Hillier, and B. D. Rainford, *Physica B* **359-361**, 983 (2005).
- ¹⁶D. L. Cox and A. Zawakowski, *Adv. Phys.* **47**, 599 (1998).
- ¹⁷E. A. Goremychkin, R. Osborn, E. D. Bauer, M. B. Maple, N. A. Frederick, W. M. Yuhasz, F. M. Woodward, and J. W. Lynn, *Phys. Rev. Lett.* **93**, 157003 (2004).
- ¹⁸K. Kuwahara, K. Iwasa, M. Kohgi, K. Kaneko, S. Araki, N. Metoki, H. Sugawara, Y. Aoki and H. Sato, *J. Phys. Soc. Jpn.* **73**, 1438 (2004).
- ¹⁹K. Kuwahara, K. Iwasa, M. Kohgi, K. Kaneko, N. Metoki, S. Raymond, M.-A. Méasson, J. Flouquet, H. Sugawara, Y. Aoki, and H. Sato, *Phys. Rev. Lett.* **95**, 107003 (2005).
- ²⁰Y. Aoki, T. Namiki, S. Ohsaki, S. R. Saha, H. Sugawara, and H. Sato, *J. Phys. Soc. Jpn.* **71**, 2098 (2002).
- ²¹Pei-chun Ho, J. Singleton, M. B. Maple, H. Harima, P. A. Goddard, Z. Henkie, and A. Pietraszko, *New J. Phys.* **9**, 269 (2007).
- ²²S. D. Wilson, P. Dai, D. T. Adroja, S.-H. Lee, J.-H. Chung, J. W. Lynn, N. P. Butch, and M. B. Maple, *Phys. Rev. Lett.* **94**, 056402 (2005).
- ²³K. Takegahara, *J. Phys. Soc. Jpn.* **69**, 1572 (2000).
- ²⁴K. Takegahara, H. Harima, and A. Yanase, *J. Phys. Soc. Jpn.* **70**, 1190 (2001).
- ²⁵K. R. Lea, M. J. M. Leask, and W. P. Wolf, *J. Phys. Chem. Solids* **23**, 1381 (1962).
- ²⁶R. J. Birgeneau, *J. Phys. Chem. Solids* **33**, 59 (1972).